13th ewtec 2019 Proceedings of the 13th European Wave and Tidal Energy Conference 1-6 Sept 2019, Naples, Italy

Evaluation of predictionless control for wave energy converters

Hancheol Cho, Giorgio Bacelli, Victor Nevarez, Felipe Wilches-Bernal, and Ryan G. Coe

***Abstract*—In this paper, a feedback control strategy for a wave energy converter (WEC) with no prediction is proposed that provides performance rivaling a prediction-based controller, even when assuming perfect prediction. This innovative control scheme is derived first by abstracting the WEC in the same structure as an electrical circuit and by applying the Jacobi's maximum power transfer law to optimize WEC power absorption. By considering the implementation of complex conjugate control problem over a finite bandwidth, a causal controller can be realized. This causal controller can be defined such that its frequency response follows that of the complex conjugate controller as closely as possible using fitting techniques such as system identification. This suboptimal controller requires no prediction and only the device velocity needs to be measured to calculate control signals. Additionally, a model predictive controller (MPC) is designed to handle constraints with minimal (1-step) prediction. In implementing this MPC, prediction of wave elevation is not required either and the standard MPC block available in the MathWorks MPC toolbox can be employed, which is of great importance for practical applications. The MPC behaves as a predesigned causal controller and also acts as a supervisory controller to prevent the device from hitting end-stops. The performance of the proposed causal controllers and the MPC is compared with the complex conjugate controller in terms of the mean power absorption and it is shown that more than 90% of the theoretical maximum can be achieved.**

***Index Terms*—Causality, Control, Wave energy converter (WEC).**

I. Introduction

It is well known that ocean waves have considerable benefits and potentials as a source of renewable energy. Wave energy provides the highest power density among renewable energy sources such as solar and wind energies. However, there are still many technical challenges in realizing the benefits of water power energy. One of the main challenges is the difficulty in converting the irregular reciprocating motion of the ocean waves into useful motion to drive a generator with acceptable output quality. Hence, active control strategies for a wave energy converter (WEC) to maximize energy extraction from ocean waves play a critical role in this sense.

Fortunately, complex conjugate (CC) control, developed in the frequency domain, is known to optimize device velocity and guarantee maximum power absorption [1]. In implementing this control strategy in practice, one issue to be overcome in real-time control is that the CC solution is noncausal, requiring a prediction for the wave elevation or the excitation force in advance. In the case of regular waves, prediction is trivial, but in real irregular waves future wave oscillations are not easily known nor estimated [2].

Nonetheless, a general assumption is made in much of the literature such that the excitation force from incoming waves can be a priori known or sufficiently accurately estimated. Various control algorithms have been proposed that utilize latching control [3], dynamic programming [4], model predictive control [5], fuzzy logic control [6], pseudospectral methods [7], and shape-based control [8]. Compared with the prediction-based control schemes listed above, causal approaches that only employ past and current measurement data such as position and velocity of the device are in general much simpler, require much less computational burden, do not suffer from prediction error, and can be implemented using the most basic of measurements. In [9], a reference velocity is calculated from the current measurement of the excitation force without prediction, which is then tuned in real time to the optimal value provided by CC control and imposed on the system to be tracked via classical control theory. It is proposed in [10] that the optimal causal controller can be determined as the solution of a nonstandard linear quadratic Gaussian problem assuming the wave excitation as a stochastic disturbance. In [11], a feedback resonating (FBR) controller based on impedance matching is proposed.

This paper presents a comparison of a number of predictionless controllers, using the noncausal CC as a reference; in theory, the CC provides an upper bound in terms of absorbed power. Additionally, the paper presents a frequency-domain tuning technique for model predictive control (MPC) which has two main advantages compared to the current implementations:

ID Number: 1527, Conference Track: Grid integration, power take-off and control

Sandia National Laboratories is a multi-mission laboratory managed and operated by National Technology and Engineering Solutions of Sandia, LLC., a wholly owned subsidiary of Honeywell International, Inc., for the U.S. Department of Energy's National Nuclear Security Administration under contract DE-NA0003525. This paper describes objective technical results and analysis. Any subjective views or opinions that might be expressed in the paper do not necessarily represent the views of the U.S. Department of Energy or the United States Government.

H. Cho is with Water Power Technologies Program, Sandia National Laboratories, Albuquerque, NM, 87185 U.S.A (e-mail: hancho@sandia.gov).

G. Bacelli is with Water Power Technologies Program, Sandia National Laboratories, Albuquerque, NM, 87185 U.S.A (e-mail: gbacell@sandia.gov).

V. Nevarez is with Advanced Fuzing Technology Program, Sandia National Laboratories, Albuquerque, NM, 87185 U.S.A (e-mail: vnevare@sandia.gov).

F. Wilches-Bernal is with Electric Power Systems Research Program, Sandia National Laboratories, Albuquerque, NM, 87185, U.S.A (fwilche@sandia.gov).

R.G. Coe is with Water Power Technologies Program, Sandia National Laboratories, Albuquerque, NM, 87185 U.S.A (e-mail: rcoe@sandia.gov).

predictions of wave elevation or excitation force are not required for power maximization; the controller can be implemented using the standard MPC block available in the MathWorks MPC toolbox. The characteristics are of great importance for practical applications because the structure of the controller is much simpler, and there is no need to implement a custom optimizer to solve the MPC problems in real-time – a task that is far from being trivial. Both the PI and MPC implementations described in this paper have been tested experimentally; the results and the link to the experimental data are provided in [12].

Ten sea states of JONSWAP type spectra are applied to produce the CC curves and to develop the corresponding controllers. It is shown that a proportional-integral (PI) type controller (assuming a first order) is optimal only in a narrow band of frequencies and a higher-order FBR controller matches the CC curve over a broader range of frequencies and guarantees higher efficiency in absorbing power from the waves. A model predictive controller (MPC) is also designed such that it behaves exactly as the designed PI or FBR controllers when constraints are inactive, while satisfying the constraints in an optimal manner when they are active. When constraints are active, MPC acts as a supervisory controller to prevent the device from hitting end-stops. The performance of the proposed PI, FBR, and MPC (with and without constraints) in terms of the mean power absorption is compared with that of the CC controller and a standard MPC with perfect prediction. Through extensive simulations, it is found that the mean power absorption obtained using the FBR controller for the ten sea states is equal to more than 90% of the theoretical maximum predicted by the non-causal CC controller.

II. Problem formulation

This paper provides an in-depth explanation of control strategies that avoid the acausality problem of a WEC. Fig. 1 shows a "hierarchy" of WEC control. Starting with the intrinsic impedance of the WEC, one can formulate the CC control, which is the optimal power transfer for a WEC [1]. As shall be shown shortly, a PI controller and a FBR controller can be designed as causal approximation of the CC control over a limited frequency range (see workflow in Fig. 1).

Then a model predictive controller (MPC) is derived from these feedback controllers to allow for constraints. Note that the MPC proposed in this paper is different from a typical MPC considered for WEC control in that the obtained intrinsic impedance data is directly utilized to avoid the need for extended wave prediction: it is essentially a frequency-domain design of an MPC. A more traditional MPC, which assumes the perfect prediction of incoming waves, is also designed in order to be compared with the other causal controllers. Each controller is explained in more detail from Section III through Section V.

Throughout the paper, a single degree of freedom heaving point absorber was selected for the case study. A diagram of the WEC device and its relevant parameter values are given in Fig. 2 and Table I, respectively.

TABLE I
Model-scale WEC physical parameters.

Parameter	Value
Rigid-body mass (float & slider), M [kg]	858
Displaced volume, $\forall$ [m^3]	0.858
Float radius, r [m]	0.88
Float draft, T [m]	0.53
Water density, ρ [kg/m^3]	1000
Water depth, h [m]	6.1
Linear hydrostatic stiffness, S [kN/m]	23.9
Infinite-frequency added mass, m_∞ [kg]	782
Max vertical travel, $\lvert z_{\max}\rvert$ [m]	0.6

Each of the controllers' performance is compared for a series of sea states, all of which are of JONSWAP type spectra and summarized in Table II.

III. Complex conjugate control and causal realizations

As noted in the previous section, CC control provides us with the theoretical maximum of the absorbed power. This section starts with a brief introduction of the CC control and its realizations are proposed in PI and FBR forms.

The equations of WEC motion are usually defined as

$$\left[i\omega(M+m(\omega))+B_v+R(\omega)+\frac{S}{i\omega}\right]v(\omega)= F_e(\omega)+F_{pto}(\omega), \quad (1)$$

where ω is the angular frequency, M is the mass matrix of the device, $m(\omega)$ is the added mass, B_v is the damping, $R(\omega)$ is the radiation damping, S is the hydrostatic restoring coefficient matrix, $v(\omega)$ is the velocity of the WEC device, $F_e(\omega)$ is the excitation force from the incoming waves, and $F_{pto}(\omega)$ is the mechanical force applied by the power take-off (PTO).

The power absorption over the entire frequency range is

$$W_{pto}=-\frac{1}{2\pi}\int_0^\infty [F_{pto}(\omega)v^*(\omega)+F^*_{pto}(\omega)v(\omega)]d\omega, \quad (2)$$

where the asterisk (*) denotes the complex conjugate of a quantity. Defining the intrinsic impedance $Z_i(\omega)$ in (1) as

$$Z_i(\omega)=i\omega(M+m(\omega))+B_v+R(\omega)+\frac{S}{i\omega}, \quad (3)$$

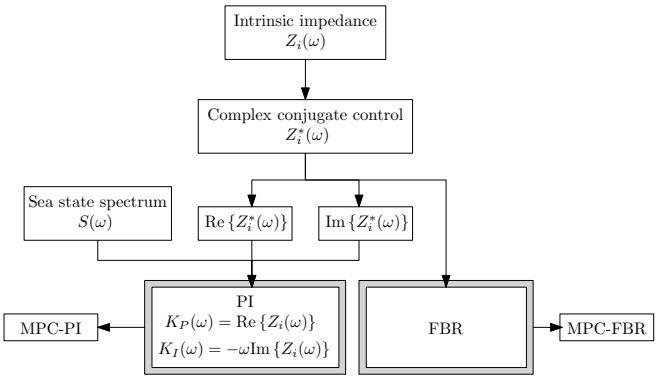

Fig. 1. Hierarchy for WEC control design.

TABLE II
LIST OF SEA STATES AND OPTIMAL CONTROLLER TUNINGS. T_p DENOTES THE PEAK PERIOD, H_s IS THE SIGNIFICANT WAVE HEIGHT, AND γ DENOTES THE PEAK ENHANCEMENT FACTOR.

Test case	T_p [s]	H_s [m]	γ	PI		P	FBR				
				K_I	K_P	K_P	$a1$	$a0$	$b2$	$b1$	$b0$
1	1.58	0.127	1	-3221.91	2412.66	2498.7	85.05	0	-76.52	91.29	-1213
2	1.58	0.127	3.3	-1636.3	2255.87	2267.88	47.66	0	-40.56	53.64	-653.7
3	2.5	0.127	1	-13748.7	2016.61	4876.61	22.81	6.766	-17.73	26.26	-285.5
4	2.5	0.127	3.3	-13097.5	1946.55	5022.55	28.68	8.652	-22.44	34.6	-355.4
5	2.5	0.254	1	-13786.3	2008.89	4881.24	22.81	6.766	-17.73	26.26	-285.5
6	2.5	0.254	3.3	-13150.59	1939.29	5030.47	28.68	8.652	-22.44	34.6	-355.4
7	3.5	0.127	1	-18510.49	1389.55	8926.72	42.7	5.577	-36.27	46.43	-570.6
8	3.5	0.127	3.3	-18042.9	1345.76	9342.9	184.5	20.79	-162.1	214.9	-2471
9	3.5	0.254	1	-18566.14	1420.61	8927.85	42.7	5.577	-36.27	46.43	-570.6
10	3.5	0.254	3.3	-18058.7	1340.85	9347.21	184.5	20.79	-162.1	214.9	-2471

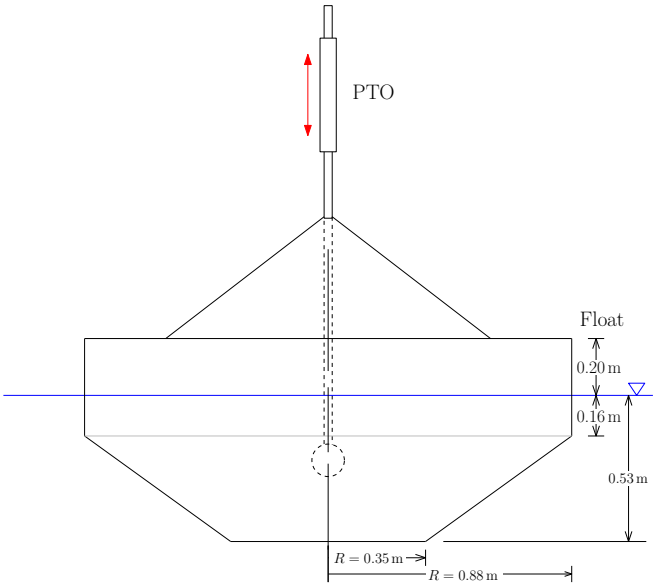

Fig. 2. Study device diagram.

one can show that when the PTO force satisfies

$$F_{pto}(\omega) = -Z_i^*(\omega)v(\omega), \tag{4}$$

the power absorption defined in (2) has its maximum [1]

$$W_{pto,MAX} = \frac{1}{2\pi}\int_0^\infty \frac{|F_e(\omega)|^2}{2R_i(\omega)}d\omega, \tag{5}$$

where $R_i(\omega)$ is the intrinsic resistance of the device that is equal to the real part of $Z_i(\omega)$.

We can see from (4) where the term complex conjugate control is originated from. It is straightforward to show that the CC controller has a noncausal property by investigating an impulse response [1]. Owing to this noncausality of the CC controller, a lot of effort has been made in the literature to predict the future behavior of the incoming waves. Instead, we will seek other methods that will accomplish causal realizations of the CC controller with only feedback action by trying to match the $Z_i^*(\omega)$ curve.

The causal realization is achieved via system identification (SID) or curve fitting. More specifically, a causal controller expressed in a transfer function form is obtained by determining the transfer function parameters that fit the complex conjugate curve as closely as possible while maintaining stability. Two causal controllers are proposed in this paper: PI and FBR controllers.

A. PI control

Let us first consider a simple case - PI control in first-order. In general, a PI control can be modeled as the following first-order system

$$U(s) = \frac{(K_P s + K_I)}{s}V(s), \tag{6}$$

where $U(s)$ and $V(s)$ are the Laplace transforms of the control force $u(t)$ and the velocity of the device $v(t)$, respectively, and K_P and K_I are constant gains to be determined.

With (3), we can write the transfer function in (6) as

$$Z_i(s) = \frac{K_P s + K_I}{s}. \tag{7}$$

Comparing (3) and (7), one can deduce the PI controller gains:

$$K_P(\omega) = \mathrm{Re}\{Z_i(\omega)\} = B_v + R(\omega) \tag{8}$$

and

$$K_I(\omega) = -\omega\,\mathrm{Im}\{Z_i(\omega)\} = -\omega^2(M + m(\omega)) + S. \tag{9}$$

From (8) and (9), it is obvious that these values can only be determined at an individual frequency. This fact is more clearly visualized in Fig. 3, where the PI controller matches the complex conjugate curve only at one point for the magnitude and phase response.

Hence, the PI controller is generally able to capture the optimality only in a small frequency band and the response error will grow outside this band. The growth of this error depends on the bandwidth of the WEC device. The optimal K_I and K_P gains that maximize the mean of mechanical power absorption are provided in Table II for each test case listed in Table II.

In this paper, a simpler proportional (P) control is considered as well for reference, which is called the damping control. This type of control contains only P gain, i.e., $K_I = 0$, and it is frequently encountered in the WEC control design, but expected to have poorer performance than PI control. The optimal P gains are summarized in Table II for each sea state.

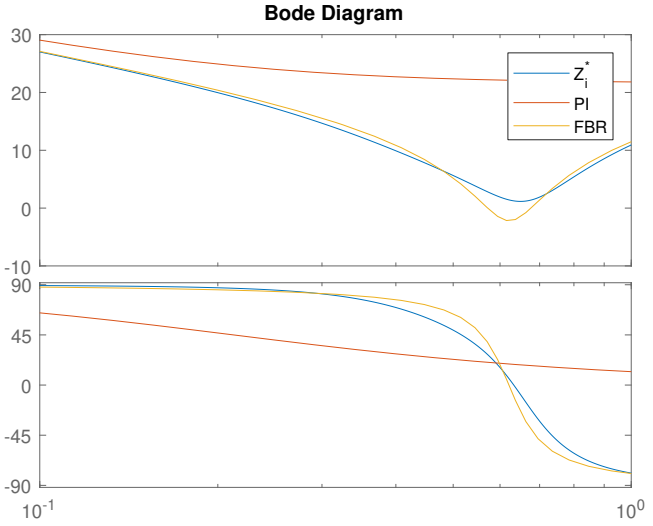

Fig. 3. Bode diagram comparing the complex conjugate controller response (Z_i^*) with stable causal realizations for PI ($f_p = 0.6667\,\text{Hz}$) and FBR controllers.

B. FBR control

As seen in the previous subsection, the PI control could match the CC curve only at one point, hence, its performance is limited. Using a higher-order model, we expect that the matching would be improved both in the magnitude and phase. Hence, we expect to see the FBR controller to outperform the PI controller for all wave spectra as seen from Fig. 3.

In this paper, the FBR controller is realized as a second-order transfer function with two poles and two zeros. More specifically, each FBR transfer function has the following form:

$$U(s) = \frac{b_2 s^2 + b_1 s + b_0}{s^2 + a_1 s + a_0} V(s). \tag{10}$$

Even with the second-order model, it is not possible to match the CC curve over the whole range of frequencies, so we rather are looking at a specific frequency range: $0.1 < f < 1.0\,\text{Hz}$, which is the relevant band for the device considered here. Using the built-in SID methods within the MATLAB System Identification Toolbox, we were able to determine the optimal coefficients in (10) for each test case that are listed in Table II.

IV. Predictionless MPC

Model predictive control (MPC) has a number of potential benefits over pure feedback control strategies (i.e., PI or FBR), such as the capability to handle constraints. Hence, in this subsection a new MPC algorithm is derived that will behave exactly as the predesigned PI or FBR controller when constraints are inactive. It will inherit favorable properties of frequency-domain linear control design and simultaneously be able to handle the constraints in an optimal manner when they are active. A more classical MPC is also developed with the assumption of perfect prediction of a wave profile and the performance of this noncausal controller will be compared with the PI, P, FBR, and matched MPC in the next section.

In [13], it was shown that a linear state-feedback controller can be realized via MPC with specially tuned weight matrices, which is called MPC matching. Since the PI and FBR controllers developed in the previous subsections are simple examples of state feedback control, we can apply this method to obtain MPC that exactly behaves as the predesigned PI or FBR controller with no prediction when constraints are inactive, thereby avoiding the acausality problem.

In MPC formulation, the following finite-horizon optimal control problem is solved at each sampling time

$$\mathcal{V}(\boldsymbol{x}(k), \boldsymbol{u}(k)) = \min_{\boldsymbol{U}(k)} \; \boldsymbol{x}'(N|k)\mathbf{P}\boldsymbol{x}(N|k) + \sum_{i=0}^{N-1} \boldsymbol{x}'(i|k)\mathbf{Q}\boldsymbol{x}(i|k) + \boldsymbol{u}'(i|k)\mathbf{R}\boldsymbol{u}(i|k) \tag{11}$$

such that

$$\boldsymbol{x}(i+1|k) = \mathbf{A}\boldsymbol{x}(i|k) + \mathbf{B}\boldsymbol{u}(i|k), \quad i = 0, ..., N-1, \tag{12}$$

$$x_{min} \le \|\boldsymbol{x}(i|k)\| \le x_{max}, \quad i = 0, ..., N, \tag{13}$$

$$u_{min} \le \|\boldsymbol{u}(i|k)\| \le u_{max}, \quad i = 0, ..., N-1, \tag{14}$$

$$\boldsymbol{x}(0|k) = \boldsymbol{x}(k), \tag{15}$$

where (12) is the discrete-time state space equation of the plant model, $\boldsymbol{x} \in \mathbb{R}^n$ is the state vector, $\boldsymbol{u} \in \mathbb{R}^m$ is the control input vector, N is the prediction horizon, $\boldsymbol{U}(k) = [\boldsymbol{u}'(0|k) \; ... \; \boldsymbol{u}'(N-1|k)] \in \mathbb{R}^{Nm}$ is the vector to be optimized, and $\mathcal{V} : \mathbb{R}^n \to \mathbb{R}_{0+}$ is the value function. The matrices $\mathbf{P} \in \mathbb{R}^{n\times n}$, $\mathbf{Q} \in \mathbb{R}^{n\times n}$, and $\mathbf{R} \in \mathbb{R}^{m\times m}$ are the weight matrices that should be tuned. Assuming that the current state $\boldsymbol{x}(k)$ is given, the finite horizon optimal control problem (11) can be recast to the following quadratic program (QP) with respect to $\boldsymbol{U}(k)$

$$\min_{\boldsymbol{U}(k)} \; \boldsymbol{U}'(k)\mathbf{H}\boldsymbol{U}(k) + 2\boldsymbol{x}'(k)\mathbf{F}\boldsymbol{U}(k) \tag{16}$$

such that

$$\mathbf{G}\boldsymbol{U}(k) \le \boldsymbol{\lambda} + \boldsymbol{\Lambda}\boldsymbol{x}(k), \tag{17}$$

where $\mathbf{G} \in \mathbb{R}^{q\times Nm}$, $\boldsymbol{\lambda} \in \mathbb{R}^q$, and $\boldsymbol{\Lambda} \in \mathbb{R}^{q\times n}$ are the problem constraints. Also, the following new matrices are defined in (16)

$$\mathbf{H} = \mathcal{R} + \mathcal{S}'\mathcal{Q}\mathcal{S}, \quad \mathbf{F} = \mathcal{T}'\mathcal{Q}\mathcal{S}, \tag{18}$$

where $\mathcal{S}$ is the N-steps state reachability matrix, $\mathcal{T}$ is the N-steps free evolution matrix

$$\mathcal{S} = \begin{bmatrix} \mathbf{B} & \mathbf{0} & \dots & \mathbf{0} \\ \mathbf{AB} & \mathbf{B} & \dots & \mathbf{0} \\ \vdots & \vdots & \ddots & \vdots \\ \mathbf{A}^{N-1}\mathbf{B} & \mathbf{A}^{N-2}\mathbf{B} & \dots & \mathbf{B} \end{bmatrix}, \quad \mathcal{T} = \begin{bmatrix} \mathbf{A} \\ \mathbf{A}^2 \\ \vdots \\ \mathbf{A}^N, \end{bmatrix}, \tag{19}$$

and $\mathcal{Q} \in \mathbb{R}^{Nn\times Nn}$, $\mathcal{R} \in \mathbb{R}^{Nm\times Nm}$ are block-diagonal matrices

$$\mathcal{Q} = \begin{bmatrix} \mathbf{Q} & \mathbf{0} & \mathbf{0} & \dots & \mathbf{0} \\ \mathbf{0} & \mathbf{Q} & \mathbf{0} & \dots & \mathbf{0} \\ \vdots & \vdots & \ddots & \vdots & \vdots \\ \mathbf{0} & \mathbf{0} & \dots & \mathbf{Q} & \mathbf{0} \\ \mathbf{0} & \mathbf{0} & \dots & \mathbf{0} & \mathbf{P} \end{bmatrix}, \quad \mathcal{R} = \begin{bmatrix} \mathbf{R} & \mathbf{0} & \dots & \mathbf{0} \\ \mathbf{0} & \mathbf{R} & \dots & \mathbf{0} \\ \vdots & \vdots & \ddots & \vdots \\ \mathbf{0} & \dots & \mathbf{0} & \mathbf{R} \end{bmatrix}. \tag{20}$$

When constraints are not active, the QP (16) has the unconstrained optimal solution $\boldsymbol{U}^*(k)$ which is given by

$$\boldsymbol{U}^*(k) = \begin{bmatrix} \boldsymbol{u}^*(0|k) \\ \vdots \\ \boldsymbol{u}^*(N-1|k) \end{bmatrix} = -\mathbf{H}^{-1}\mathbf{F}'\boldsymbol{x}(k). \tag{21}$$

The MPC command at step k then picks up only the first move such that

$$\boldsymbol{u}_{\mathrm{MPC}}(\boldsymbol{x}(k)) = \boldsymbol{u}^*(0|k) = -\boldsymbol{\Gamma}\mathbf{H}^{-1}\mathbf{F}'\boldsymbol{x}(k), \tag{22}$$

where $\boldsymbol{\Gamma} = [\mathbf{I}_m \;\; \mathbf{0} \;\; \dots \;\; \mathbf{0}]$.

Now, we consider a predesigned linear controller in a state feedback form

$$\boldsymbol{u}_{\mathrm{LN}}(k) = \mathbf{K}\boldsymbol{x}(k), \quad \mathbf{K} \in \mathbb{R}^{m\times n}. \tag{23}$$

Then, the objective is to find weight matrices $\mathbf{P}$, $\mathbf{Q}$, and $\mathbf{R}$ in (11) such that

$$-\boldsymbol{\Gamma}\mathbf{H}^{-1}\mathbf{F}' = \mathbf{K}, \tag{24}$$

where $\mathbf{K}$ is given.

In brief, once the weight matrices $\mathbf{P}$, $\mathbf{Q}$, and $\mathbf{R}$ are found that satisfy (24) given $\mathbf{K}$, then the MPC with the cost function (11) behaves as the linear controller of the form (23), when the constraints are not active. More specifically, when the gain matrix $\mathbf{K}$ that is composed of the optimal gains provided in Table II and II, the weight matrices $\mathbf{P}$, $\mathbf{Q}$, and $\mathbf{R}$ used in $\mathbf{H}$ and $\mathbf{F}$ in (18)-(20) are calculated using a numerical optimizer such that the norm of the matrix $\boldsymbol{\Gamma}\mathbf{H}^{-1}\mathbf{F}' + \mathbf{K}$ is minimized from (24). The prediction horizon $N = 2$ is employed and the control horizon is set as the same as the prediction horizon because shorter horizon requires less computational loads and the control performance is independent of N in an unconstrained application [13]. On the other hand, when constraints are active, a short horizon might degrade the control performance due to inaccurate prediction. However, in this paper, even for constrained cases, the prediction horizon $N = 2$ is applied because good performance is still observed as will be shown in the next section. Use of longer prediction horizon will be handled in future work and the obtained control results such as the control forces, velocities of the device, and the mean power capture will be shown in the next section.

V. MPC WITH PREDICTIONS

This section describes the implementation of MPC requiring prediction of the excitation force as proposed in [14] ("traditional" MPC). The design of the controller begins with the definition of the continuous-time state space model for the WEC described in Section II,

$$\begin{aligned} \dot{\boldsymbol{x}}_c(t) &= \mathbf{A}_c\boldsymbol{x}_c(t) + \mathbf{B}_c(u_c(t) + v_c(t)), \\ \boldsymbol{y}_c(t) &= \mathbf{C}_c\boldsymbol{x}_c(t), \end{aligned} \tag{25}$$

where $u_c(t)$ is the PTO force per unit mass and $v_c(t)$ is the excitation force per unit mass. Here, the state vector $\boldsymbol{x}_c$ and the output vector $\boldsymbol{y}_c$ are defined, respectively, as

$$\boldsymbol{x}_c = \begin{bmatrix} z \\ \dot{z} \\ \boldsymbol{x}_r \end{bmatrix} \in \mathbb{R}^{2+n}, \qquad \boldsymbol{y}_c = \begin{bmatrix} z \\ \dot{z} \end{bmatrix} \in \mathbb{R}^2, \tag{26}$$

where n is the order of the radiation subsystem model. The vertical position of the device is denoted by z and $\boldsymbol{x}_r \in \mathbb{R}^n$ is the state vector of radiation dynamics. The matrices $\mathbf{A}_c$, $\mathbf{B}_c$ and $\mathbf{C}_c$ are [14]

$$\mathbf{A}_c = \begin{bmatrix} 0 & 1 & \mathbf{0} \\ \frac{-S}{M+m_\infty} & \frac{-B_v}{M+m_\infty} & \frac{-1}{M+m_\infty}\mathbf{C}_r \\ \mathbf{0} & \mathbf{B}_r & \mathbf{A}_r \end{bmatrix} \in \mathbb{R}^{(n+2)\times(n+2)}, \tag{27}$$

$$\mathbf{B}_c = \begin{bmatrix} 0 \\ 1 \\ \mathbf{0} \end{bmatrix} \in \mathbb{R}^{(n+2)\times 1}, \qquad \mathbf{C}_c = \begin{bmatrix} 1 & 0 & \mathbf{0} \\ 0 & 1 & \mathbf{0} \end{bmatrix} \in \mathbb{R}^{2\times(n+2)}, \tag{28}$$

where S is the hydrostatic restoring coefficient, B_v is a linear damping term describing the viscous effects of the fluid (and/or any other linear friction terms), M is the mass of the buoy and m_∞ is the asymptotic value of the added mass. For the parameter values refer to Table I. The matrices $\mathbf{A}_r$, $\mathbf{B}_r$ and $\mathbf{C}_r$, as usual, describe the dynamics of the radiation force (f_r):

$$\begin{aligned} \dot{\boldsymbol{x}}_r(t) &= \mathbf{A}_r\boldsymbol{x}_r(t) + \mathbf{B}_r\dot{z}(t), \\ f_r(t) &= \mathbf{C}_r\boldsymbol{x}_r, \end{aligned} \tag{29}$$

where

$$\mathbf{A}_r = \begin{bmatrix} -3.9913 & -2.6621 \\ 4 & 0 \end{bmatrix}, \mathbf{B}_r = \begin{bmatrix} 64 \\ 0 \end{bmatrix}, \quad \mathbf{C}_r = \begin{bmatrix} 104.4457 & 0 \end{bmatrix}. \tag{30}$$

To be used by an MPC, the continuous-time dynamic model (25) should be reformulated in discrete time. Following [14], the discretization of the model in (25) is carried out by means of a first order-hold, yielding

$$\boldsymbol{x}(k+1) = \mathbf{A}\,\boldsymbol{x}(k) + \mathbf{B}\,\Delta u(k+1) + \mathbf{F}\,\Delta v(k+1), \tag{31}$$

$$\boldsymbol{y}(k) = \mathbf{C}\,\boldsymbol{x}(k), \tag{32}$$

where $\Delta u(k+1) = u_d(k+1) - u_d(k)$ and $\Delta v(k+1) = v_d(k+1) - v_d(k)$. Here, u_d and v_d denote the sampled versions of u_c and v_c, respectively, and

$$\mathbf{A} = \begin{bmatrix} \boldsymbol{\phi}(h) & \boldsymbol{\Gamma} & \boldsymbol{\Gamma} \\ \mathbf{0} & 1 & 0 \\ \mathbf{0} & 0 & 1 \end{bmatrix} \in \mathbb{R}^{(n+4)\times(n+4)}, \quad \mathbf{B} = \begin{bmatrix} \boldsymbol{\Lambda} \\ 1 \\ 0 \end{bmatrix} \in \mathbb{R}^{(n+4)\times 1}, \tag{33}$$

$$\mathbf{F} = \begin{bmatrix} \boldsymbol{\Lambda} \\ 0 \\ 1 \end{bmatrix} \in \mathbb{R}^{(n+4)\times 1}, \quad \mathbf{C} = \begin{bmatrix} 1 & 0 & 0 & \dots & 0 & 0 & 0 \\ 0 & 1 & 0 & \dots & 0 & 0 & 0 \\ 0 & 0 & 1 & \dots & 0 & 0 & 0 \end{bmatrix} \in \mathbb{R}^{3\times(n+4)}. \tag{34}$$

Here, $\boldsymbol{\phi}(h) = e^{\mathbf{A}_c h}$, where h is the update interval and

$$\boldsymbol{\Gamma} = \mathbf{A}_c^{-1}\left(\boldsymbol{\phi}(h) - \mathbf{I}\right)\mathbf{B}_c \;\in \mathbb{R}^{(n+2)\times 1}, \tag{35}$$

$$\boldsymbol{\Lambda} = \frac{1}{h}\mathbf{A}_c^{-1}\left(\boldsymbol{\Gamma} - h\,\mathbf{B}_c\right) \;\in \mathbb{R}^{(n+2)\times 1}. \tag{36}$$

VI. RESULTS

To compare all of the previous methods discussed, each method was tested against ten different wave cases with varying peak period and wave height. The integration time step is set to 0.005 (s) and the simulation duration is 628 (s) that is equal to the period of the incoming waves. Power capture for tested controllers in each wave profile is shown in TABLE III. Since the CC controller is the analytical maximum power capture for the particular WEC device for each wave profile, each method will compare its power capture with the theoretical maximum. The "traditional" MPC method with perfect prediction is marked as MPC-PP. From TABLE III, we can see that the MPC-PP controller most closely approximates the CC controller. However, the PI and FBR controllers are not far behind - recall the relative simplicity of implementing these controllers compared to the MPC with perfect prediction.

The FBR controller performs quite well. In the worst case, when the wave peak period ($f_p = 0.2857\,\text{Hz}$) is far from the device resonant frequency ($f_p = 0.6667\,\text{Hz}$) (test cases #7-10). Due to this, any frequency band that does not expand out to the resonant frequency will not properly capture the device dynamics. To accommodate for this the frequency band needs to cover a larger frequency band and even with this issue, the FBR controller performed within one percent of the MPC perfect prediction controller.

We see that the MPC-PI and MPC-FBR controllers match the PI and FBR controllers closely. For example, let us measure the performance by FIT (%) - the mean square error between the MPC-PI and PI control signals:

$$FIT = (1 - NRMSE) \times 100, \tag{37}$$

where the term $NRMSE$ is defined as

$$NRMSE = \frac{\|u_{\text{PI}} - u_{\text{MPC}}\|_2}{\|u_{\text{PI}} - \bar{u}_{\text{PI}}\|_2}, \tag{38}$$

where u_{PI} is the control signal (force) created by the PI controller, $\bar{u}_{\text{PI}}$ is the mean value of u_{PI}, and u_{MPC} is the control signal calculated by the MPC-PI controller. For example, the FIT is calculated as 99.64% for test case #10, which verifies that the obtained MPC-PI behaves as the PI controller pretty well. Also, it is seen that the designed MPC-FBR controller behaves almost exactly like the FBR controller. More specifically, the FIT of the MPC-FBR control signal is calculated as 99.35% compared with that of the FBR controller for test case #10.

Fig. 4 display the power spectral density obtained by the CC, PI, FBR, and P (damping) controllers for test cases #1, #2, #5, #6, #9, and #10, respectively. As seen from Fig. 4, all the controllers make a similar shape with the wave profile; the power is absorbed the most at the frequency at which the wave force has its peak. Also, the power captured by the CC lies in a broader range of frequencies than the other controllers, especially in low frequencies . The FBR shares a similar shape with the CC and the PI captures a little less power than the CC or the FBR. The P controller absorbs the least amount of power. As expected, the waves with smaller γ have a broader range of frequencies, and hence, the corresponding controllers absorb power from this broad frequency band. For example, compare test case #5 ($\gamma = 1$) with test case #6 ($\gamma = 3.3$).

In order to clearly see that the FBR controller covers a broader range of frequencies than the PI or the P controllers, Fig. 4 is reused to plot the power ratio; the power captured by the PI, FBR, and P controllers is divided by the power captured by the CC controller (theoretical maximum) for each frequency. The results are presented in Fig. 5, clearly showing that the FBR captures almost as much power as the CC, from a broader range of frequencies than the PI or the P controllers. The efficiency of the PI controller is high only in a narrow frequency band and the P controller absorbs the least power among the three. For reference, the wave spectrum which has the legend '$J/max\{J\}$' for each test case is displayed. Due to the narrow-banded nature of the wave energy profile the PI controller with only two parameters can successfully absorb wave energy near the peak frequency and the FBR controller with a larger bandwidth can extract even more energy.

Fig. 6a shows the time history of the control signals for test case #10 created by the MPC with perfect prediction (PP), PI, and FBR controllers. It is seen that the three control signals are in phase on the whole. More specifically, the MPC with PP and the FBR controller share a similar profile and have a little larger amplitudes, compared with the PI controller. In Fig. 6b the time history of the velocities of the buoy for test case #10 obtained by the MPC with PP, PI, and FBR controllers is depicted. Again, the MPC with PP and FBR controller have a similar velocity profile compared with the PI controller. Fig. 6c displays the time history of the mechanical power for test case #10 captured by using the MPC with PP, PI, and FBR controllers. Again, the MPC with PP and FBR controller share a similar power capture profile together, supporting the finding that the average power captured by the MPC with PP is commensurate with that captured by the FBR controller (see TABLE III). The MPC-PI and MPC-FBR controllers yield almost the same results with the PI and FBR controllers, respectively, so their results are not shown here for brevity.

Now, the MPC-PI and the MPC-FBR controllers with the saturation constraint on the control force (we call it MPC-PI-CON and MPC-FBR-CON respectively) are designed and their performance is provided. It is shown that the power captured by the MPC-PI-CON and the MPC-FBR-CON is poor only by a small amount when compared with the unconstrained MPC-PI and MPC-FBR even though a short horizon $N = 2$ is employed. For both controllers (MPC-PI-CON and MPC-FBR-CON), the control force signal is saturated within the range [-10000 10000] (N).

First, to compare unconstrained/constrained MPC-PI, Fig. 7a shows the time history of the control signals generated by the PI, MPC-PI, and MPC-PI-CON controllers for test case #10. It is seen from the figures that the constraint is well satisfied and the three curves almost overlap with each other when the

TABLE III
POWER CAPTURE COMPARISON (POWER SHOWN IN WATTS).

Test Case	CC	P	MPC-PP	PI	FBR	MPC-PI	MPC-FBR
1	3.6	2.9	3.4	2.9	3.5	2.9	3.5
2	4.0	3.4	3.8	3.4	3.8	3.4	3.8
3	18.4	8.3	17.4	15.4	17.4	15.4	17.4
4	20.5	9.4	19.4	17.9	19.4	17.9	19.4
5	73.6	33.1	69.5	62.0	70.0	61.8	70.0
6	81.9	37.9	77.5	72.0	78.0	71.8	78.2
7	71.0	13.9	66.4	57.1	65.8	56.7	65.8
8	77.7	15.3	72.8	65.3	72.3	64.9	72.0
9	284.2	55.6	265.9	225.4	259.5	223.9	259.5
10	310.7	61.2	290.5	262.0	290.4	260.3	289.3

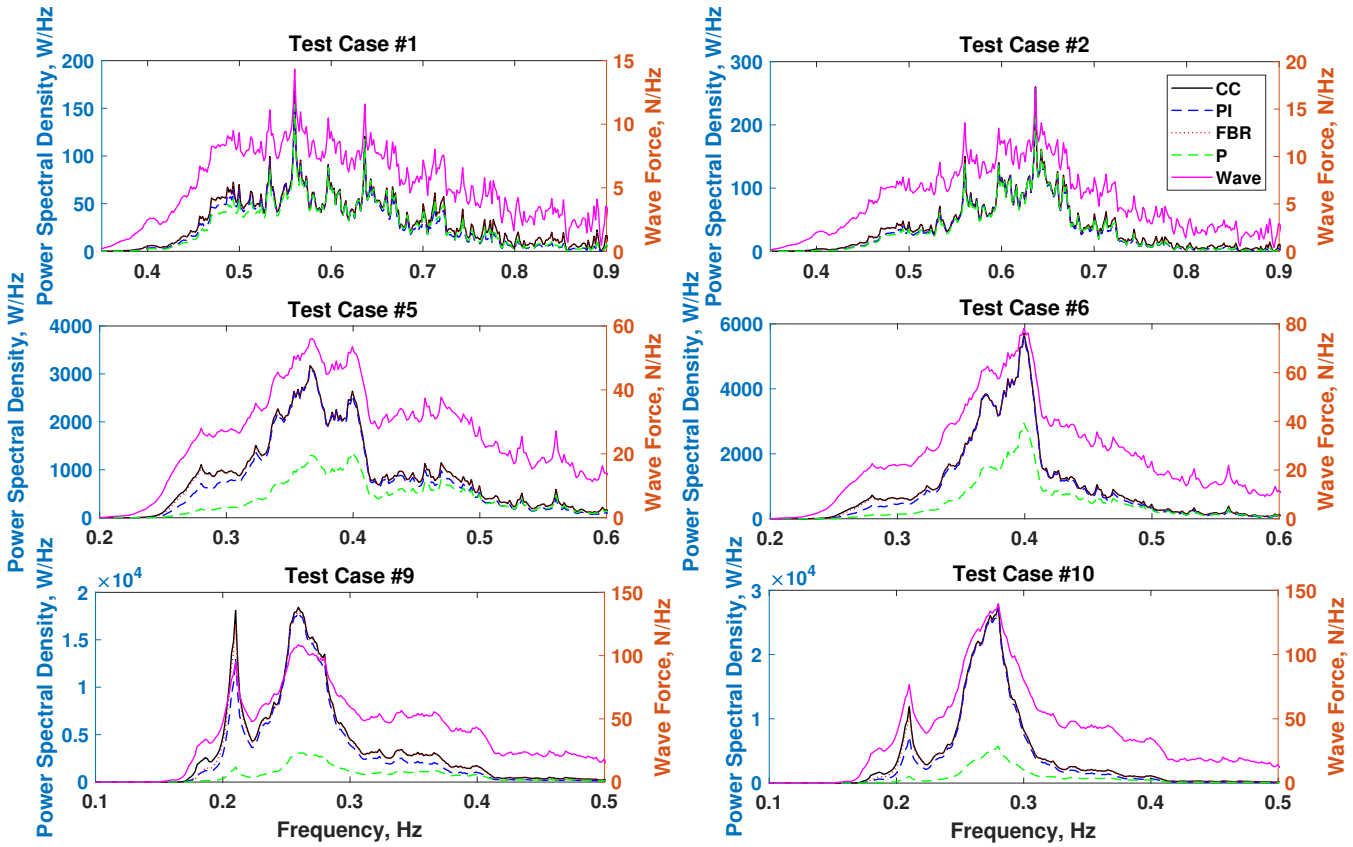

Fig. 4. Power spectral density obtained by CC, PI, FBR, and P controllers.

constraint is not active. In Fig. 7b, the time history of the velocities of the buoy obtained by the PI, MPC-PI, and MPC-PI-CON controllers is depicted. Since the control signal of the MPC-PI mimics the PI control signal pretty well, their resulting velocities are also quite similar. Also, we can see that the MPC-PI-CON yields a smaller velocity than the others when the control signal is saturated. Fig. 7c displays the time history of the mechanical power captured by using the PI, MPC-PI, and MPC-PI-CON controllers. As expected, when the constraint is active, the power is less captured than when the constraint is inactive. More specifically, the power captured by each controller is 261.99 W (PI), 260.26 W (MPC-PI), and 241.37 W (MPC-PI-CON), indicating that the performance of the MPC-PI-CON is reduced by 7.26% when compared with the unconstrained MPC-PI.

Likewise, the performance of the FBR, MPC-FBR, and MPC-FBR-CON is compared for test case #10, and the control signal is again saturated within the range [-10000 10000] (N). It is seen from Fig. 8a that the constraint is well satisfied and the three curves overlap with each other when the constraint is inactive. In Fig. 8b, the time history of the velocities of the buoy obtained by the FBR, MPC-FBR, and MPC-FBR-CON controllers is depicted. It is again found that the MPC-FBR-CON yields a smaller velocity when the control signal is saturated. Fig. 8c displays the time history of the mechanical power captured by using the FBR, MPC-FBR, and MPC-FBR-CON controllers. As expected, less power is captured when the constraint is active. More specifically, the power captured by each controller is 290.39 W (FBR), 289.32 W (MPC-FBR), and 269.25 W (MPC-FBR-CON), indicating that the performance of the MPC-FBR-CON is reduced by 7.09% when compared with the MPC-FBR.

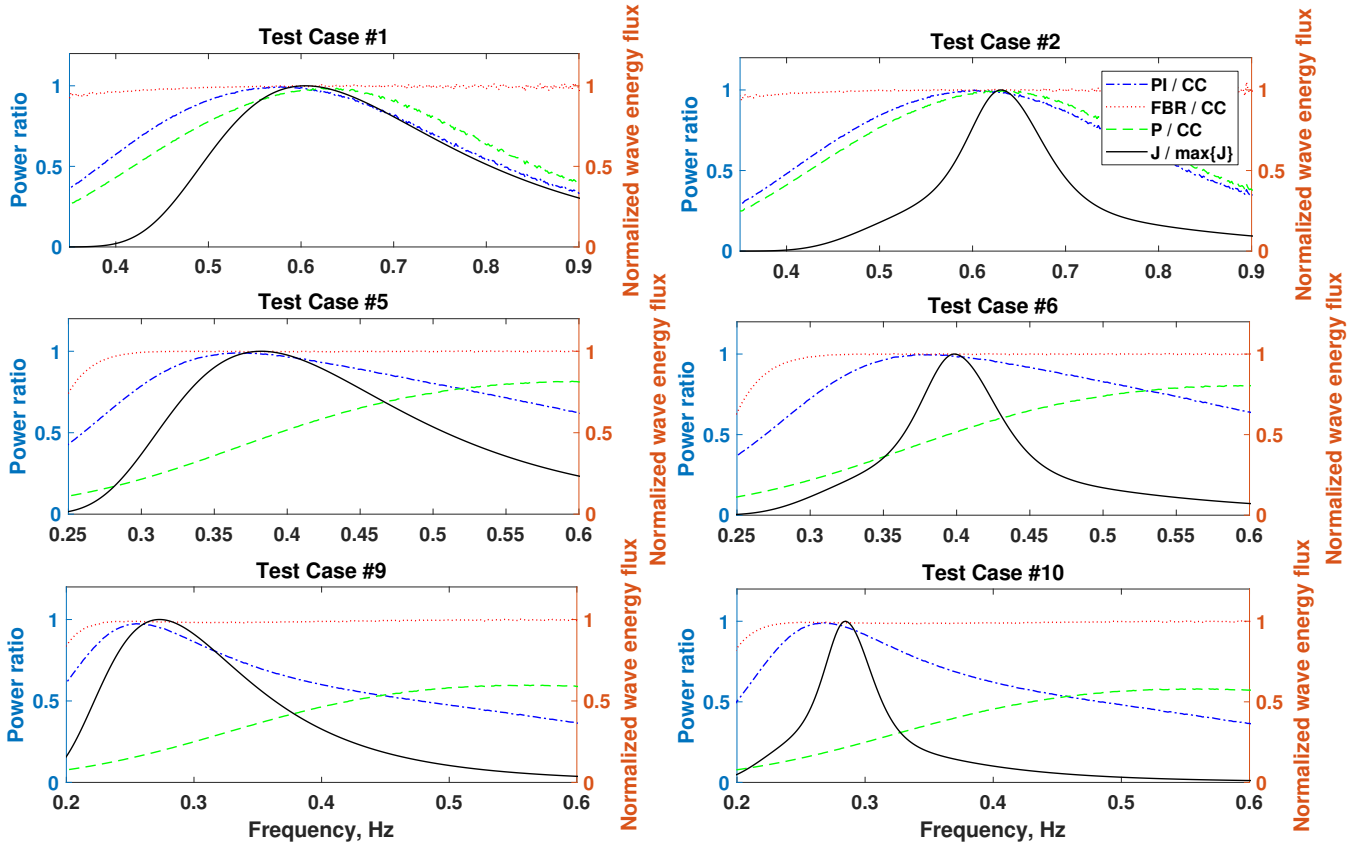

Fig. 5. Power ratio divided by the power captured by CC.

VII. Conclusion

This paper studies a key question in wave energy control research: the need for and benefit of wave prediction. As we can see from comparing the causal realization methods to the complex conjugate control and the standard MPC methods, the performance of the causal realization methods is commensurate with that of the standard MPC with perfect prediction. The major benefit to using these causal realization methods is that there is no prediction involved with determining these controllers. Due to the removal of the prediction strain, there is less dependence and the computational strain of estimating and optimizing over a particle wave history to a device. The causal predictionless controllers derived also could be realized via MPC technique with specially tuned weight matrices. The MPC is readily implemented using the existing MPC toolbox and performs supervisory control that respects system constraints. In brief, given this consideration, the feedback-only controllers (PI, FBR, MPC-PI, MPC-FBR, MPC-PI-CON, and MPC-FBR-CON) have impressive benefits of its own and provide commensurate performance to prediction-based control without the need for a prediction of future wave excitation.

References

[1] J. Falnes, *Ocean Waves and Oscillating Systems*. Cambridge; New York: Cambridge University Press, 2002.

[2] U. Korde, "Control system applications in wave energy conversion," in *OCEANS 2000 MTS/IEEE Conference and Exhibition*, vol. 3, 2000, pp. 1817–1824 vol.3.

[3] A. Babarit and A. Clement, "Optimal latching control of a wave energy device in regular and irregular waves," *Applied Ocean Research*, vol. 28, no. 2, pp. 77–91, Apr. 2006. [Online]. Available: http://www.sciencedirect.com/science/article/pii/S0141118706000423

[4] G. Li, G. Weiss, M. Mueller, S. Townley, and M. R. Belmont, "Wave energy converter control by wave prediction and dynamic programming," *Renewable Energy*, vol. 48, pp. 392–403, Dec. 2012. [Online]. Available: http://www.sciencedirect.com/science/article/pii/S0960148112003163

[5] J. Hals, J. Falnes, and T. Moan, "Constrained optimal control of a heaving buoy wave-energy converter," *Journal of Offshore Mechanics and Arctic Engineering*, vol. 133, no. 1, pp. 1–15, 2011.

[6] M. Schoen, J. Hals, and T. Moan, "Robust control of heaving wave energy devices in irregular waves," in *2008 16th Mediterranean Conference on Control and Automation*, Jun. 2008, pp. 779–784.

[7] G. Bacelli, J. Ringwood, and J.-C. Gilloteaux, "A control system for a self-reacting point absorber wave energy converter subject to constraints," in *Proceedings of 18th IFAC World Congress*, Milan, Italy, Aug. 2011. [Online]. Available: http://eprints.nuim.ie/3555/

[8] O. Abdelkhalik, R. Robinett, S. Zou, G. Bacelli, R. Coe, D. Bull, D. Wilson, and U. Korde, "On the control design of wave energy converters with

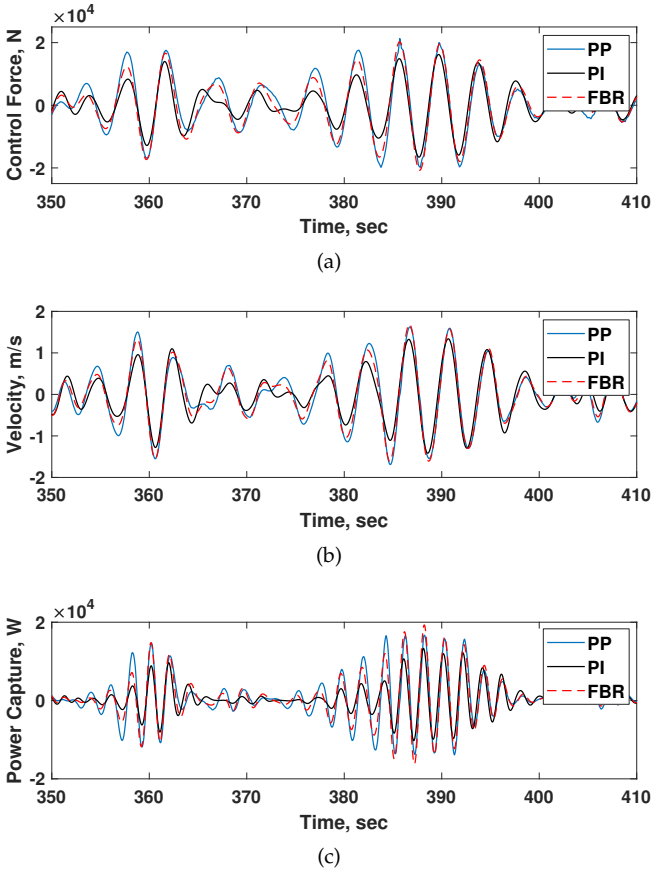

Fig. 6. MPC with PP, PI, and FBR controllers for test case #10.

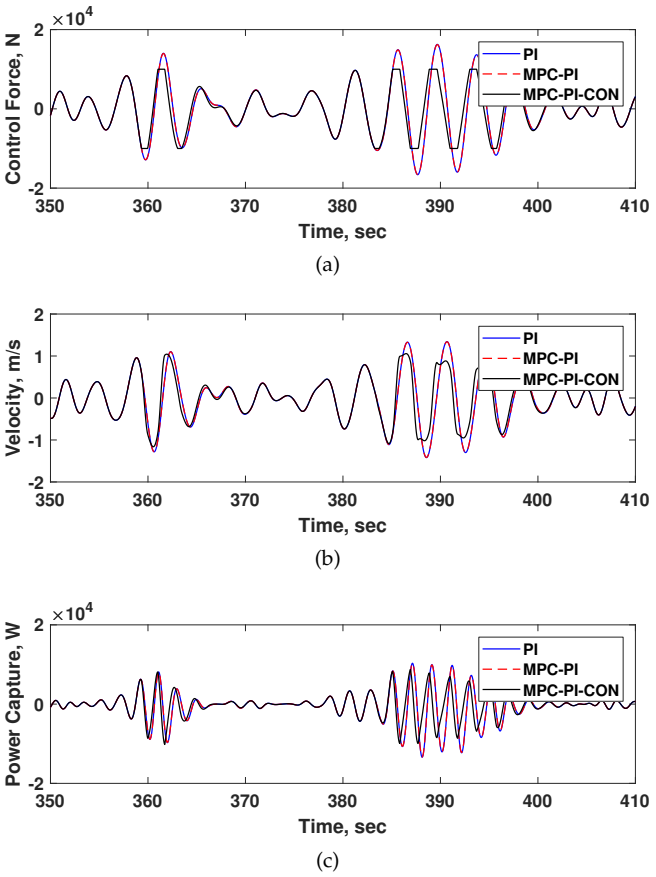

Fig. 7. PI, MPC-PI, and MPC-PI-CON controllers for test case #10.

wave prediction," *Journal of Ocean Engineering and Marine Energy*, vol. 2, no. 4, pp. 473–483, 2016. [Online]. Available: http://dx.doi.org/10.1007/s40722-016-0048-4

[9] F. Fusco and J. Ringwood, "A simple and effective real-time controller for wave energy converters," *IEEE Transactions on Sustainable Energy*, vol. 4, no. 1, pp. 21–30, Jan. 2013.

[10] J. T. Scruggs, S. M. Lattanzio, A. A. Taflanidis, and I. L. Cassidy, "Optimal causal control of a wave energy converter in a random sea," *Applied Ocean Research*, vol. 42, pp. 1–15, Aug. 2013. [Online]. Available: http://www.sciencedirect.com/science/article/pii/S0141118713000205

[11] V. Nevarez, G. Bacelli, R. G. Coe, and D. G. Wilson, "Feedback resonating control for a wave energy converter," in *Proceedings of SPEEDAM2018*, 2018.

[12] R. G. Coe, G. Bacelli, S. J. Spencer, and H. Cho, "Initial results from wave tank test of closed-loop wec control," Albuquerque, NM, 2018.

[13] S. D. Cairano and A. Bemporad, "Model predictive control tuning by controller matching," *IEEE Transactions on Automatic Control*, vol. 55, no. 1, pp. 185–190, Jan 2010.

[14] J. A. M. Cretel, G. Lightbody, G. P. Thomas, and A. W. Lewis, "Maximisation of energy capture by a wave-energy point absorber using model predictive control," in *IFAC World Congress*, 2011.

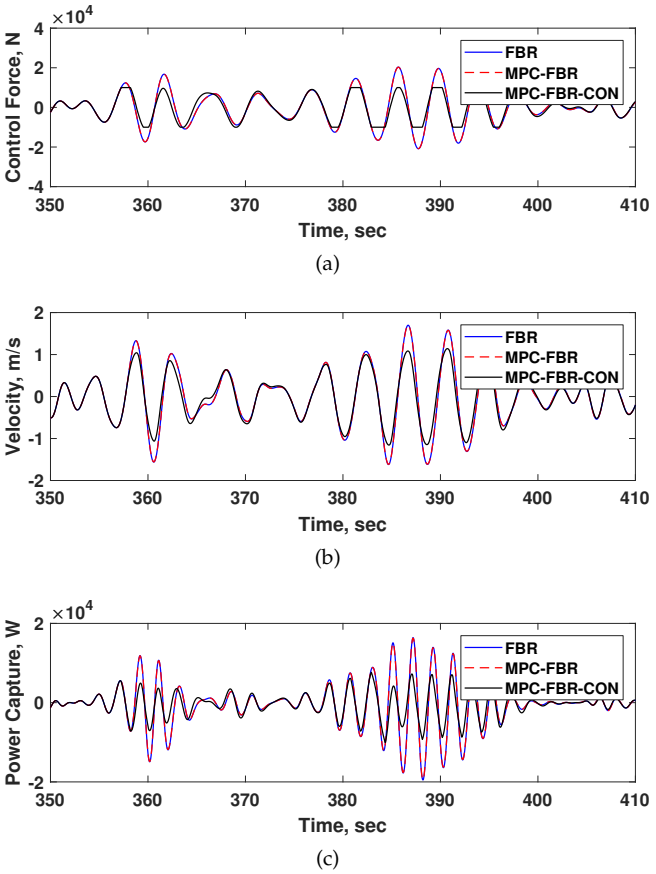

Fig. 8. FBR, MPC-FBR, and MPC-FBR-CON controllers for test case #10.